Nanocrystalline Silicon Hot Paper

DOI: 10.1002/ange.201411830

Preparation of Nanocrystalline Silicon from $SiCl_4$ at 200 °C in Molten Salt for High-Performance Anodes for Lithium Ion Batteries**

Ning Lin, Ying Han, Liangbiao Wang, Jianbin Zhou, Jie Zhou, Yongchun Zhu, and Yitai Qian**

Abstract: *Crystalline Si nanoparticles are prepared by reduction of $SiCl_4$ with metallic magnesium in the molten salt of $AlCl_3$ at 200 °C in an autoclave. $AlCl_3$ not only acts as molten salt, but also participates in the reaction. The related experiments confirm that metallic Mg reduces $AlCl_3$ to create nascent Al which could immediately reduce $SiCl_4$ to Si, and the by-product $MgCl_2$ would combine with $AlCl_3$ forming complex of $MgAl_2Cl_8$. As anode for rechargeable lithium ion batteries, the as-prepared Si delivers the reversible capacity of 3083 mAh g^{-1} at 1.2 A g^{-1} after 50 cycles, and 1180 mAh g^{-1} at 3 A g^{-1} over 500 cycles.*

Over the past half century, silicon has been applied in various fields, such as electric devices, photovoltaic devices, and biosensors.[1] Recently, Si materials have also been considered as the promising anode candidates for rechargeable lithium ion batteries (LIBs) owing to their high theoretical capacity (3579 mAh g^{-1}) and relatively low discharge potential (< 0.5 V versus Li/Li$^+$).[2] For example, Si nanowires fabricated by decomposing silanes showed discharge capacity of 3500 mAh g^{-1} at 0.84 Ag^{-1} for 20 cycles.[3]

Traditionally, Si materials were synthesized from silica, such as carbothermic reduction at above 2000 °C,[4] magnesiothermic reduction at about 650 °C,[5] and electrochemical reduction in molten salts (> 850 °C).[6] Previously, our group prepared Si nanoparticles by reducing silica sol with Mg in 180 °C hydrothermally.[7]

And also, Si nanomaterials were commonly obtained starting from silicon tetrachloride ($SiCl_4$).[8] In 1940s, the Dupont company established a method to prepare polycrystalline Si through gas-phase reduction of $SiCl_4$ with Zn at 1000 °C. In 1950s, Zn was replaced by H_2 at 1200 °C, developed by Alcatel–Lucent Bell Labs.

In 1992, Heath et al. firstly synthesized crystalline Si in hexane through reduction of $SiCl_4$ with metallic Na at 385 °C in a steel bomb for 3–7 days.[9] Subsequently, NaSi or KSi was utilized as reductant to react with $SiCl_4$ in organic solvents at room temperature, leading to the formation of nanosized Si.[10] However, the obtained Si was not fully crystallized.[11] Recently, a similar method based on organic solution route has been exploited for synthesizing nanostructured Si as anode for LIBs.[11,12] Jaephil Cho and et al. synthesized Si nanoparticles, followed by annealing treatment and carbon coating, exhibiting high specific charge capacity of 3535 mAh g^{-1} at 0.9 A g^{-1} and retention as 96% after 40 cycles.[11]

Herein, we report the preparation of nanocrystalline Si from $SiCl_4$ reduced by metallic Mg at 200 °C in molten salt of $AlCl_3$ (m.p. 190 °C). However, without $AlCl_3$, the direct reaction between metallic Mg and $SiCl_4$ could not be initiated at 200 °C. To understand the reaction process, several related experiments were carried out. At 200 °C, metallic Mg powder can reduce $AlCl_3$ to create metallic Al. Therefore, it is proposed that the created nascent Al in the above reaction system could immediately reduce $SiCl_4$ to Si. Meanwhile, the by-product of $MgCl_2$ could combine with $AlCl_3$ and form complex metal chlorides of $MgAl_2Cl_8$. So, it can be seen that $AlCl_3$ plays dual roles in promoting the reaction to progress at low temperature, which not only acts as molten salt, but also participates in the reaction. Overall, the reaction in the reduction process can be expressed as Reaction 1:

$$2\,Mg + SiCl_4 + 4\,AlCl_3 \rightarrow MgAl_2Cl_8 + Si \quad (1)$$

When used as anode for rechargeable LIBs, the as-prepared Si nanoparticles deliver high reversible capacity of 3083 mAh g^{-1} at 1.2 A g^{-1} after 50 cycles, and 1180 mAh g^{-1} at 3 A g^{-1} over 500 cycles.

The XRD pattern of the final sample is shown in Figure 1 a. All five peaks at 28.56, 47.44, 56.25, 69.3, and 76.51° are indexed to the diffraction peaks of cubic Si (JCPDS 27-1402). Base on Sherrer's equation, the size of the Si particles are estimated to be about 30 nm. The XRD pattern of the sample without hydrofluoric acid (HF) treatment

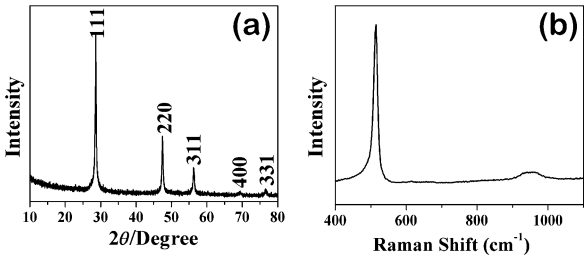

Figure 1. a) XRD patterns and b) Raman spectrum of the as-prepared Si sample.

[*] N. Lin, Y. Han, L. B. Wang, J. B. Zhou, J. Zhou, Dr. Y. C. Zhu, Prof. Y. t. Qian
Department of Chemistry and Hefei National Laboratory for Physical Science at Micro-scale
University of Science and Technology of China
Hefei, Anhui 230026, (P. R. China)
E-mail: ychzhu@ustc.edu.cn
ytqian@ustc.edu.cn

[**] We gratefully acknowledge support from the 973 Project of China (No. 2011CB935901) and the National Natural Science Fund of China (No. 91022033, 21201158, 21471142).

Supporting information for this article is available on the WWW under http://dx.doi.org/10.1002/anie.201411830.

shows no obvious difference (Supporting Information, Figure S1). Furthermore, the Raman spectrum (Figure 1b) of the sample after HF treatment exhibits a clear peak at 513 cm^{-1}, corresponding to first-order Raman scattering from optic phonons of Si–Si stretching motions of Si. Furthermore, the broad peaks located at around 955 cm^{-1} are assigned to the overtones of TO (L).[13]

SEM (Figure 2a) and TEM (Figure 2b) images exhibit that the obtained Si sample consists of polycrystalline nanoparticles with the overall size ranging from several tens to about 100 nm. The enlarged TEM picture inserted in Figure 2b shows that the Si particles are composed of inter-

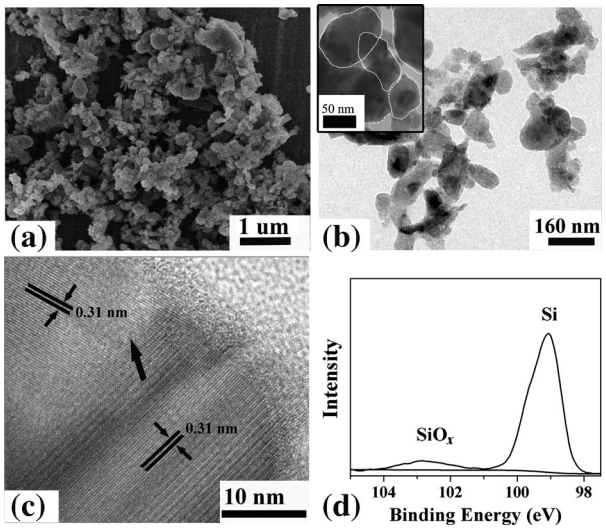

Figure 2. a) SEM, b) TEM, c) HRTEM images, and d) XPS spectrum of the prepared Si sample.

connected Si grains. The HRTEM image, shown in Figure 2c, reveals lattice fringe images of the Si nanocrystals. Two clearly interplanar distances are all measured to be about 0.31 nm, corresponding to the (111) crystal planes of the cubic Si. Clearly, a grain boundary is observed, which may be resulted from the interconnected crystalline Si grains. Owing to the disordered arrangement of the atoms in grain boundary, the crystal structure is relatively loose, which would serve as a fast diffusion path of electrons/lithium ions. Commonly, the disordered atom arrangement is associated with vacancy and dislocation that are generally favorable for improving the conductivity. Furthermore, the surface contents of the Si nanoparticles are investigated by X-ray photoelectron spectroscopy (XPS) spectrum, as shown in Figure 2d. A dominant peak at about 100 eV indicates the existence of Si. A weak peak at 103.5 eV, attributed to Si^{4+}, may correspond to small amount of amorphous SiO_x.[14] Compared with the sample before HF treatment, it was shown that the silicon oxides formed during exposure of the Si nanocrystals to the air atmosphere have been selectively dissolved (Supporting Information, Figure S2).

To understand the reaction process of preparing crystalline Si, a series of related experiments were carried out. The raw products of the proposed Reaction (1) without any

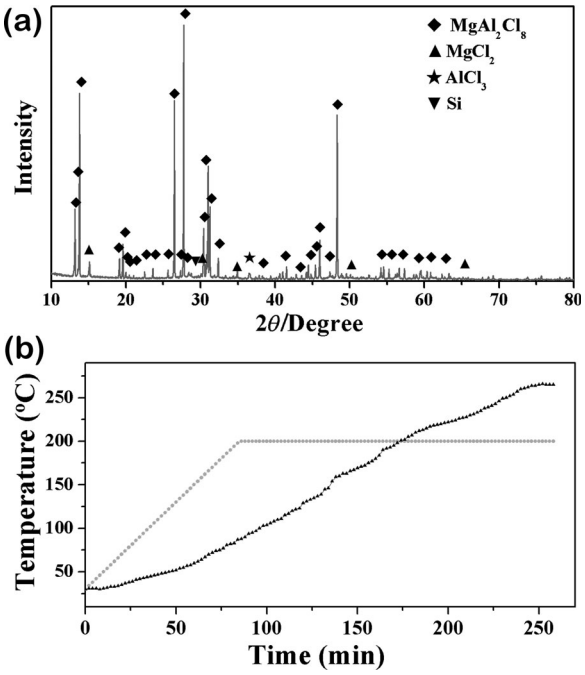

Figure 3. a) XRD patterns of the obtained raw product without any washing treatment. b) The temperature change plots as a function of time inside the electric furnace (●, gray) and inside the stainless steel autoclave (▲, black).

further washing treatment were collected and analyzed by XRD immediately (Figure 3a). Clearly, a group of extremely strong diffraction peaks (labeled as ◆) in the pattern are characterized as $MgAl_2Cl_8$ (JCPDS No.78-0916), which is supposed to be the main by-product. The existence of $MgCl_2$ (labeled as ▲ JCPDS No. 72-1517) is attributed to the excess product. It should be pointed out that a very weak peak at 36.6° may be a small quantity of residual $AlCl_3$ (labeled as ⋆ JCPDS No. 77-0819). Only a feature diffraction peak at 28.5° is detected, which may be caused by the larger amount of well-crystallized salts generated in the system.[15]

The related experiments show that metallic Mg is capable of reacting with $AlCl_3$ at 200 °C. The corresponding XRD patterns (Supporting Information, Figure S3) exhibit that the products consist of $MgAl_2Cl_8$, $MgCl_2$, and metallic Al. Based on the above investigation, it is proposed that $AlCl_3$ would participate in the reaction system running as the following steps. First, the nascent Al* is created by reduction of $AlCl_3$ with metallic Mg:

$$3\,Mg + 2\,AlCl_3 = 3\,MgCl_2 + 2\,Al^* \quad (2)$$

Then, these in situ created, highly chemically active Al*, which contact closely with $SiCl_4$ under atomic scale in liquid environment, can reduce $SiCl_4$ to Si immediately:

$$4\,Al^* + 3\,SiCl_4 = 4\,AlCl_3 + 3\,Si \quad (3)$$

However, commercial Al powder is unable to reduce $SiCl_4$ even at 500 °C. Owing to the higher chemical activity of the Al* than bulk Al, reaction of $SiCl_4$ with the nascent Al* is

therefore prone to be initiated. Finally, the eutectic compound of $MgAl_2Cl_8$ is formed in the system:

$$MgCl_2 + 2\,AlCl_3 \rightleftharpoons MgAl_2Cl_8 \quad (4)$$

The temperature inside the stainless steel autoclave during the reaction was also measured (Figure 3b). As the temperature of the electric furnace rises to 200 °C steadily following the pre-set program, the inner temperature increases slowly to 200 °C at first, then reaches up to 265 °C. Meanwhile, according to the calculation of the free energy, Reaction (1) is thermodynamically spontaneous and highly exothermic. As a result, the autogenic heat, which results in higher local temperature, further facilitates the reaction progress and the crystallization of Si. Overall, the added $AlCl_3$ not only acts as molten salt providing a liquid environment, but also participates in the reaction, which is favorable for the formation of the well-crystallized Si at low temperature of 200 °C. Ideally, the by-products of metal chlorides could be easily removed by water.

The discharge–charge voltage profiles of the as-prepared crystalline Si nanoparticles at a current density of 0.3 g^{-1} are shown in Figure 4a. In the first cycle, a distinct discharge voltage plateau at around 0.1 V (vs. Li/Li^+) is observed, which arises from the Li–Si alloying reaction between Li^+ and

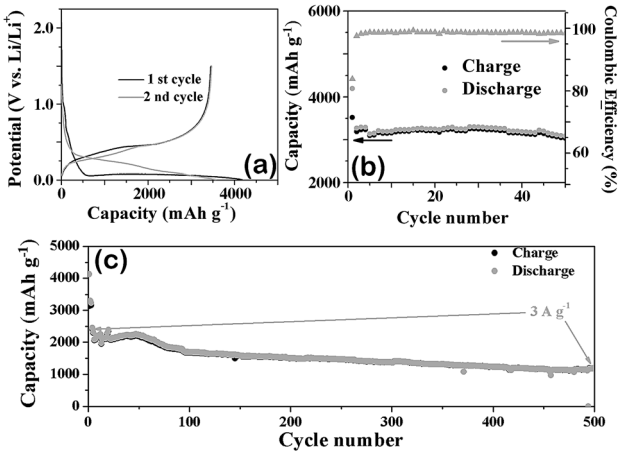

Figure 4. a) Discharge–charge voltage curves and b), c) cycling behavior tested at b) 1.2 A g^{-1} and c) 3 A g^{-1} for the as-prepared crystalline Si nanoparticles.

crystalline Si.[16] From second cycle forward, the discharge potential plateau of first cycle is replaced by a sloping curve owing to the amorphization of Si, which is consistent with the CV curves (Supporting Information, Figure S4). Notably, the first discharge and charge capacity are 3549 and 4189 mAh g^{-1}, respectively. The corresponding initial coulombic efficiency is as high as 84.7 %, which is significant for practical applications. The irreversible capacity is most likely caused by the formation of solid electrolyte interface (SEI), and the side reactions between Si and the electrolyte (especially $LiPF_6$).[17]

Next, the cycling reversible capacity of the as-prepared Si nanoparticles is monitored by galvanostatic charge/discharge tests in the voltage range of 0.005–1.50 V. As shown in Figure 4b, the Si nanoparticles deliver a reversible capacity as high as 3083 mAh g^{-1} at 1.2 A g^{-1} over 50 cycles. Despite the capacity degradation within the first two cycles caused by generation of SEI, the reversible capacity of the Si electrode retains 94.28 % of the second discharge capacity after 50 cycles. It is significant that the corresponding coulombic efficiency quickly increases to 97.4 % for the second cycle and then reaches a steady value over 98 % after several cycles.

The long-term cycling stability at high current density electrode was also studied (Figure 4c). It should be mentioned that the cells are tested at a relative low current density of 0.3 A g^{-1} for first three cycles to activate the anode sufficiently.[18] The Si electrode delivers a specific capacity of 1180 mAh g^{-1} at 3 A g^{-1} after 500 cycles, with a capacity decay rate of 0.1 % per cycle from third to 500th cycle. Overall, the enhanced electrochemical performance of the prepared crystalline Si nanoparticles is attributed to the following advantageous aspects. First, the well-crystallized Si composed of interconnected nanoparticles could alleviate the large strain caused by repeated lithium ion insertion/extraction from the electrode, thus maintaining the electrical and structural integrity of the electrode. What is more, the basic nanostructured Si grain, accompanied with the grain boundary, is beneficial for decreasing the transport/diffusion path of electrons/lithium ions and further improving the conductivity. The corresponding electrochemical impedance spectroscopy (EIS) data (Supporting Information, Figure S5) show that the layer resistance in the electrode/electrode interface is relatively low.

In summary, crystalline Si nanoparticles were prepared from $SiCl_4$ in the molten salt of $AlCl_3$ at 200 °C in an autoclave. It was demonstrated that nascent Al, generated by reducing $AlCl_3$ with metallic Mg, would immediately reduce $SiCl_4$ to Si. Thus, $AlCl_3$ not only serves as molten salts, but also participates in the reaction. As anode for rechargeable lithium ion battery, the as-prepared crystalline Si nanoparticles exhibit high reversible capability and long-term cycling stability and high initial columbic efficiency. As the reaction condition is relatively mild, and the yield of the products is over 80 %, this work is applicable for mass production of Si anode materials. Moreover, our work, as a typical molten-salt reaction, develops the inorganic molten-salt reaction in low temperatures and can be extended to prepare other functional nanomaterials.

Experimental Section

All reagents were used without further purification. $SiCl_4$ was purchased from Energy Chemical Co. The other chemical reagents were purchased from Sinopharm Chemical Reagent Co. Ltd. In a typical procedure, $AlCl_3$ (5.00 g) and magnesium powder (0.84 g) were mixed and loaded in a stainless steel autoclave (volume 20 mL). Subsequently, $SiCl_4$ (2 mL) was added into the autoclave. The above procedure is conducted in a glove-box filled with N_2. Then, the autoclave was sealed immediately and heated in an electric stove with a heating ramp rate of 2 °C min^{-1} and maintained at 200 °C for 10 h. After cooling to room temperature naturally, the precipitate was collected and washed with 0.1 M hydrochloric acid, distilled water, and ethanol. The obtained sample was immersed in diluted ethanol-based

hydrofluoric acid (HF) solution for 30 min. Finally, the product was dried in vacuum at 50 °C for 10 h for further characterization. The detailed procedure of structural characterization and electrochemical measurements are exhibited in Supporting Information.

Received: December 9, 2014
Published online: February 4, 2015

Keywords: lithium ion batteries · molten salts · nanocrystalline Si · reduction of $SiCl_4$

[1] a) K. Q. Peng, J. J. Hu, Y. J. Yan, Y. Wu, H. Fang, Y. Xu, S. T. Lee, J. Zhu, *Adv. Funct. Mater.* **2006**, *16*, 387 – 394; b) U. Zywietz, A. B. Evlyukhin, C. Reinhardt, B. N. Chichkov, *Nat. Commun.* **2014**, *5*, DOI: 10.1038/ncomms4402; c) F. Lin, D. Nordlund, T. C. Weng, Y. Zhu, C. M. Ban, R. M. Richards, H. L. Xin, *Nat. Commun.* **2014**, *5*, DOI: 10.1038/ncomms4358; d) Y. P. He, F. Sui, S. S. M. Kauzlarich, G. Galli, *Energy Environ. Sci.* **2014**, *7*, 2598 – 2602.

[2] a) M. T. Mcdowell, S. W. Lee, W. D. Nix, Y. Cui, *Adv. Mater.* **2013**, *25*, 4966 – 4985; b) C. Wang, H. Wu, Z. Chen, M. T. McDowell, Y. Cui, Z. N. Bao, *Nat. Chem.* **2013**, *5*, 1042 – 1048; c) Q. Z. Xiao, Q. Zhang, Y. Fan, X. H. Wang, R. A. Susantyoko, *Energy Environ. Sci.* **2014**, *7*, 2261 – 2268.

[3] C. K. Chan, H. L. Peng, G. Liu, K. Mcilwrath, X. F. Zhang, R. A. Huggins, Y. Cui, *Nat. Nanotechnol.* **2008**, *3*, 31 – 35.

[4] M. Nagamori, I. Malinsky, A. Claveau, *Metall. Trans. B* **1986**, *17*, 503 – 514.

[5] a) A. Xing, J. Zhang, Z. H. Bao, Y. F. Mei, A. S. Gordin, K. H. Sandhage, *Chem. Commun.* **2013**, *49*, 6743 – 6745; b) H. Wu, G. Chan, J. W. Choi, I. Ryu, Y. Yao, M. T. McDowell, S. W. Lee, A. Jackson, Y. Yang, L. Hu, Y. Cui, *Nat. Nanotechnol.* **2012**, *7*, 310 – 315.

[6] J. Zhao, J. Li, P. Ying, W. Zhang, L. Meng, C. Li, *Chem. Commun.* **2013**, *49*, 4477 – 4479.

[7] J. W. Liang, X. N. Li, Y. C. Zhu, C. Guo, Y. T. Qian, *Nano Res.* **2014**, DOI: 10.1007/s12274-014-0633-6.

[8] C. S. Yang, R. A. Bley, S. M. Kauzlarich, H. W. H. Lee, G. R. Delgado, *J. Am. Chem. Soc.* **1999**, *121*, 5191 – 5195.

[9] J. R. Heath, *Science* **1992**, *258*, 1131 – 1133.

[10] a) R. A. Bley, S. M. Kauzlarich, *J. Am. Chem. Soc.* **1996**, *118*, 12461 – 12462; b) D. Mayeri, B. L. Phillips, M. P. Augustine, S. M. Kauzlarich, *Chem. Mater.* **2001**, *13*, 765 – 770.

[11] H. Kim, M. Seo, M. H. Park, J. Cho, *Angew. Chem. Int. Ed.* **2010**, *49*, 2146 – 2149; *Angew. Chem.* **2010**, *122*, 2192 – 2195.

[12] F. Dai, R. Yi, M. L. Gordin, S. Chen, D. Wang, *RSC Adv.* **2012**, *2*, 12710 – 12713.

[13] R. P. Wang, G. W. Zhou, Y. L. Liu, S. H. Pan, H. Z. Zhang, D. P. Yu, Z. Zhang, *Phys. Rev. B* **2000**, *61*, 16827 – 16832.

[14] Z. Bao, M. R. Weatherspoon, S. Shian, Y. Cai, P. D. Graham, S. M. Allan, G. Ahmad, M. B. Dickerson, B. C. Church, Z. Kang, H. W. Abernathy III, C. J. Summers, M. Liu, K. H. Sandhage, *Nature* **2007**, *446*, 172 – 175.

[15] F. Dai, J. T. Zai, R. Yi, M. L. Gordin, H. Sohn, S. Chen, D. H. Wang, *Nat. Commun.* **2014**, *5*, DOI: 10.1038/ncomms4605.

[16] Z. L. Zhang, Y. H. Wang, W. F. Ren, Q. Q. Tan, Y. F. Chen, H. Li, Z. Y. Zhong, F. B. Su, *Angew. Chem. Int. Ed.* **2014**, *53*, 5165 – 5169; *Angew. Chem.* **2014**, *126*, 5265 – 5269.

[17] J. H. Cho, S. T. Picraux, *Nano Lett.* **2014**, *14*, 3088 – 3095.

[18] N. Lin, J. B. Zhou, Y. C. Zhu, Y. T. Qian, *J. Mater. Chem. A* **2014**, *2*, 19604 – 19608.